Cell Research (2009) 19:625-637.

www.nature.com/cr

ORIGINAL ARTICLE

From the Gla domain to a novel small-molecule detector of apoptosis

Avi Cohen[1, *], Anat Shirvan[1, *], Galit Levin[1], Hagit Grimberg[1], Ayelet Reshef[1], Ilan Ziv[1]

[1]*Aposense Ltd, 5-7 Ha'Odem St, Kiryat Matalon, PO Box 7119, Petach Tikva, Israel*

Apoptosis plays a pivotal role in the etiology or pathogenesis of numerous medical disorders, and thus, targeting of apoptotic cells may substantially advance patient care. In our quest for novel low-molecular-weight probes for apoptosis, we focused on the uncommon amino acid γ-carboxyglutamic acid (Gla), which plays a vital role in the binding of clotting factors to negatively charged phospholipid surfaces. Based on the alkyl-malonic acid motif of Gla, we have developed and now present ML-10 (2-(5-fluoro-pentyl)-2-methyl-malonic acid, MW=206 Da), the prototypical member of a novel family of small-molecule detectors of apoptosis. ML-10 was found to perform selective uptake and accumulation in apoptotic cells, while being excluded from either viable or necrotic cells. ML-10 uptake correlates with the apoptotic hallmarks of caspase activation, Annexin-V binding and disruption of mitochondrial membrane potential. The malonate moiety was found to be crucial for ML-10 function in apoptosis detection. ML-10 responds to a unique complex of features of the cell in early apoptosis, comprising irreversible loss of membrane potential, permanent acidification of cell membrane and cytoplasm, and preservation of membrane integrity. ML-10 is therefore the most compact apoptosis probe known to date. Due to its fluorine atom, ML-10 is amenable to radiolabeling with the ^{18}F isotope, towards its potential future use for clinical positron emission tomography imaging of apoptosis.

***Keywords*:** molecular imaging, apoptosis, Gla domain, plasma membrane potential, cellular acidification

Cell Research (2009) **19**:625-637. doi: 10.1038/cr.2009.17; published online 17 February 2009

Introduction

There is considerable evidence indicating an important role for apoptosis in the etiology or pathogenesis of disease. Molecular detection of this fundamental 'cell suicide' process may therefore be very useful in clinical practice, assisting in diagnosis or staging of disease, monitoring of the course of disease, or early assessment of efficacy of treatment. Positron emission tomography (PET) has emerged as the leading modality for molecular imaging, enabling sensitive and quantitative assessment of cellular processes. Current approaches for *in vivo* detection of apoptosis are mostly based on large proteins or peptides, *e.g.*, Annexin-V [1], C2A domain of synaptotagmin-I [2], or caspase substrates [3, 4], which have limitations such as low clearance rate, suboptimal biodistribution or potential immunogenicity. No PET tracer for apoptosis is currently available for clinical use. Our objective was to address this need by developing novel, low molecular weight apoptosis-detectors, potentially suitable to serve as PET tracers.

Annexin-V and the C2A domain of synaptotagmin-I are used as apoptosis-probes due to their ability to bind to anionic phospholipid surfaces, in relation with the apoptosis-related externalization of phosphatidylserine (PS). Another class of proteins that bind to anionic membranes is the γ-carboxyglutamic-acid (Gla)-domain proteins, including the clotting factors II, VII, IX, and X, the

*These two authors contributed equally to this work.

Correspondence: Avi Cohen
Tel: +972-3-9215717; Fax: +972-3-9215714
E-mail: avi@aposense.com

Abbreviations: ML-10 (2-(5-fluoro-pentyl)-2-methyl-malonic acid); Gla (γ-carboxyglutamic acid); Anti-Fas (Anti-Fas antibody); PMD (plasma membrane depolarization); pH_{int} (intracellular pH); pH_{ext} (extracellular pH); PET (positron emission tomography); PS (phosphatidylserine); TMRE (tetramethylrhodamine-ethyl ester); LDH (lactate dehydrogenase); DDC (didansyl-L-cystine); HBS (Hepes buffered saline solution); HBSNa (HBS with 140 mM Na^+); HBSK (HBS with 140 mM K^+); zVAD (Z-Val-Ala-Asp-fluoromethyl ketone); $[K^+]_{ext}$ (extracellular potassium concentration); PI (propidium iodide); TB (trypan blue)

Received 16 July 2008; revised 7 October 2008; accepted 7 November 2008; published online 17 February 2009

anticoagulant proteins C and S [5], and the anti-apoptotic protein gas6 [6]. However, these proteins or their related domains have not yet been explored as potential apoptosis probes. For all these proteins, membrane binding is mediated by a domain rich in the uncommon amino acid Gla, synthesized post-translationally in the liver by γ-carboxylation of glutamate [7]. The functional importance of this carboxylation is demonstrated by the effect of oral anticoagulant drugs such as warfarin, which function by inhibiting γ-carboxylation, thus abolishing membrane binding and respective catalysis of the coagulation cascade [8]. These lines of evidence point at the alkyl-malonate group of Gla as a potential critical structural moiety, enabling binding to cells with anionic phospholipid surfaces. We therefore hypothesized that alkyl-malonate could serve as a potential building block for novel small-molecule probes for apoptosis.

Based on this hypothesis and on our previous experience in developing fluorescent small-molecule apoptosis probes of the *ApoSense* family, such as didansyl-L-cystine (DDC) [9, 10, 11] and NST-732 [12], we now present ML-10 (2-(5-fluoro-pentyl)-2-methyl-malonic acid), as a rationally designed molecule, with an amphipathic compact structure (MW=206 Da). We also describe the performance of this novel Gla-derived probe as a detector of apoptosis, and its mechanism of action.

Results

Considerations in the design of ML-10

ML-10 (Figure 1) was rationally designed, based on the alkyl-malonate motif, with the modifications required to support its potential future use as a detector of apoptosis *in vivo* with PET. The molecular design of ML-10 therefore comprised the following steps: (1) attachment of an alkyl chain to render the molecule amphipathic for membrane interaction; (2) optimization of the alkyl-chain length to five carbon atoms, based on pharmacokinetic considerations; (3) attachment of a methyl group at the α-position to block metabolism *in vivo*; and (4) attachment of a fluorine atom, towards potential future radiolabeling with the ^{18}F radio-isotope for PET. These modifications were guided, in part, by our experience gained in the development of fluorescent apoptosis probes of the *ApoSense* family.

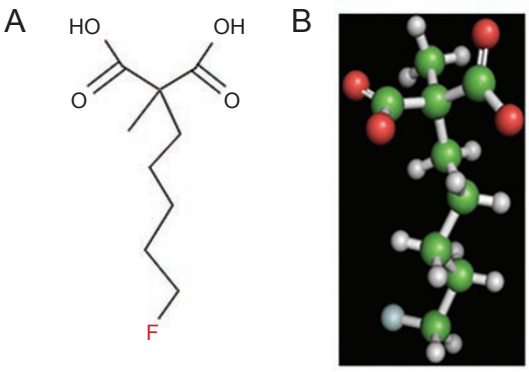

Figure 1 (A) Structure of ML-10 (2-(5-fluoro-pentyl)-2-methyl-malonic-acid). **(B)** Three-dimensional model of ML-10 in its di-anionic form. Carbon atoms are in green, oxygen atoms in red, hydrogen atoms in white and the fluorine atom in light blue.

Selective detection of apoptosis by ML-10

To test ML-10 as an apoptosis detector, we utilized a tritium-labeled derivative (^{3}H-ML-10). Cultured Jurkat cells were induced to undergo apoptosis by treatment with anti-Fas antibody (Anti-Fas) [13]. As shown in Figure 2A, control, untreated cells manifested low levels of ^{3}H-ML-10 uptake. However, upon induction of apoptosis, a nearly 10-fold increase in tracer uptake was observed. Interestingly, this uptake was not calcium-dependent, since there was no calcium in the medium. Uptake of ^{3}H-ML-10 was totally blocked by concomitant treatment with the pan-caspase inhibitor, zVAD. The increase in ^{3}H-ML-10 uptake was time-dependent (Figure 2B), respective of the progression of the apoptotic process, being minimal up to 30 min after initiation of exposure to the apoptotic trigger, reaching a maximum at 180 min after apoptosis induction, and maintaining a steady state thereafter. By contrast, ^{3}H-ML-10 uptake by the control viable cells was minimal and did not increase up to 6 h post incubation. These data demonstrate ^{3}H-ML-10 as an apoptosis-sensitive probe, manifesting selective and caspase-dependent uptake into cells undergoing apoptosis.

Similar results were obtained in utilizing a fluorescent ML-10 analog, comprising a dansyl group. Cells were co-stained with both ML-10-dansyl and propidium iodide (PI), serving as a marker for membrane disruption. While no uptake of ML-10-dansyl or PI was observed by the control viable cells (Figure 2C), exposure to the apoptotic trigger caused numerous cells to manifest ML-10-dansyl uptake (turquoise fluorescence), yet excluding PI (red fluorescence, Figure 2D). This indicates uptake of ML-10-dansyl upon induction of apoptosis, at a stage wherein membrane integrity is still preserved. This feature was also observed with tritium-labeled ^{3}H-ML-10, in which induction of apoptosis was associated with ^{3}H-ML-10 uptake, yet with the exclusion of PI or trypan blue (TB) (Figure 2E). Importantly however, ^{3}H-ML-10 uptake occurred in parallel to Annexin-V binding (Figure 2E), indicating externalization of PS on the membrane surface. We then explored subcellular localization of ^{3}H-

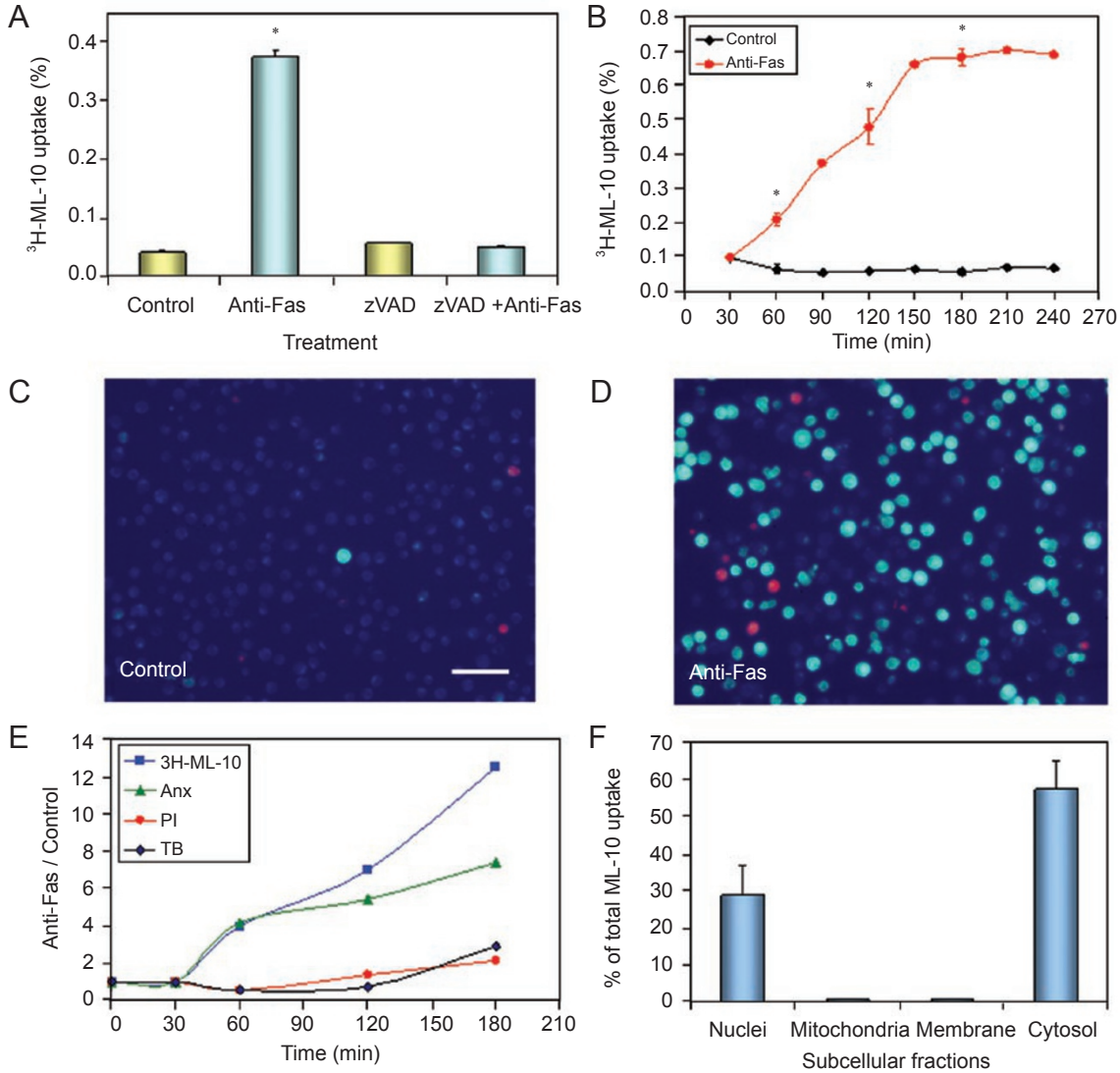

Figure 2 ^{3}H-ML-10 as a selective marker for apoptosis. **(A)** Jurkat cells were incubated with Anti-Fas in the presence or absence of the pan-caspase inhibitor zVAD-fmk for 180 min, ^{3}H-ML-10 was added for the last 60 min of incubation and its uptake was determined, mean±SD. **(B)** Time course of ^{3}H-ML-10 uptake by the apoptotic cells. **(C** and **D)** Uptake of ML-10-dansyl and propidium iodide (PI) by control **(C)** and apoptotic **(D)** Anti-Fas-treated cells. **(E)** Time course of ^{3}H-ML-10 uptake upon induction of apoptosis by Anti-Fas versus Annexin-V, PI or trypan blue (TB). **(F)** Subcellular localization of ^{3}H-ML-10 in apoptotic Jurkat cells. Data in **B**, **E**, and **F** represent the mean values obtained from the sum of three independent experiments. Scale bar = 50 μM, $*P < 0.005$.

ML-10 in the apoptotic cells, utilizing a differential centrifugation technique [14] to separate the different subcellular fractions and to determine the relative ^{3}H-ML-10 levels. ^{3}H-ML-10 was found to localize predominantly in the cytoplasm (60%). Thirty percent of ^{3}H-ML-10 was localized in the nucleus, while only traces were found in the membrane or in the mitochondrial fractions (Figure 2F). Taken together, these results indicate that while ^{3}H-ML-10 is excluded from viable cells, it evidently crosses the plasma membrane early upon apoptosis induction, with predominant subsequent accumulation in the cytoplasm and the nucleus. The crossing of the plasma membrane by ^{3}H-ML-10 occurs at the stage of early apoptosis, wherein PS exposure takes place, as indicated by the positive Annexin-V binding, while membrane integrity is still preserved, as evident by the exclusion of PI and TB.

ML-10 accumulates in apoptotic but not in necrotic cells

Interestingly, PI-positive dying cells did not accumulate ML-10-dansyl (Figure 2D). Since disruption

Table 1 ^{3}H-ML-10 accumulates in apoptotic but not in necrotic cells

Type of assay	Control cells	Apoptotic cells	Necrotic cells
^{3}H-ML-10 uptake (%)	0.049±0.004	0.392±0.049*	0.028±0.014
Caspase-3 activity (pmol/min/10^{7} cells)	8±2.8	403.3±5.8*	8.3±0.6
LDH activity in the supernatant	0.054±0.000	0.063±0.004	0.781±0.183*

Apoptosis was induced in Jurkat cells by treatment with Anti-Fas, and necrotic cell death was induced by three freeze and thaw cycles. ^{3}H-ML-10 uptake, caspase-3 activity in the cell lysate, and LDH activity in the supernatant were determined. Each value is the mean±SD of triplicate determinations from one representative experiment out of three. *$P < 0.001$ compared to control cells.

of membrane integrity, as detected by PI, is one of the hallmarks of necrotic cell death and distinguishes it from apoptosis, this feature of ML-10 demonstrates its ability to distinguish between these two modes of cell death. Such distinction is desirable and is currently not provided by other apoptosis detectors, such as Annexin-V. To further examine this feature, we compared the uptake of ^{3}H-ML-10 in two models of cell death: apoptosis versus necrosis. Necrosis was induced by freeze-thaw injury [15]. Caspase-3 activity was measured for verification of apoptosis, while LDH release was measured for assessment of necrosis, reflecting the associated membrane disruption. As shown in Table 1, induction of apoptosis by treatment with Anti-Fas was indeed associated with marked caspase activation, without concomitant LDH leakage, while the freeze-thaw injury was associated with the necrotic features of LDH release without caspase activation. Importantly, accumulation of ^{3}H-ML-10 was observed only in apoptotic cells and not in either control cells or necrotic cells (Table 1). These findings demonstrate that ML-10 is capable of distinguishing between apoptosis and necrosis, and indicate that preservation of membrane integrity by apoptotic cells, while being compromised in necrotic cells, plays a role in this distinction.

Detection of apoptosis by ML-10 probe is universal

We then examined the general utility of the probe, i.e., that it works in other cell lines and with other apoptotic stimuli. For this purpose, in addition to the above model of Anti-Fas-induced apoptosis in Jurkat cells, we also examined the performance of ML-10-dansyl in HeLa (human cervix carcinoma) cells and in CT26 (murine colon carcinoma) cells, triggered to undergo apoptosis by cisplatin or taxotere, respectively. As shown in Figure 3, also in these cell lines from diverse origins, ML-10-dansyl was excluded from control, untreated viable cells (Figure 3A and 3C). In contrast, induction of apoptosis by the chemotherapeutic agents was associated with selective and marked uptake of the probe (Figure 3B and 3D). In addition, uptake of the probe was found to be highly correlated with the binding of Annexin-V (exemplified in

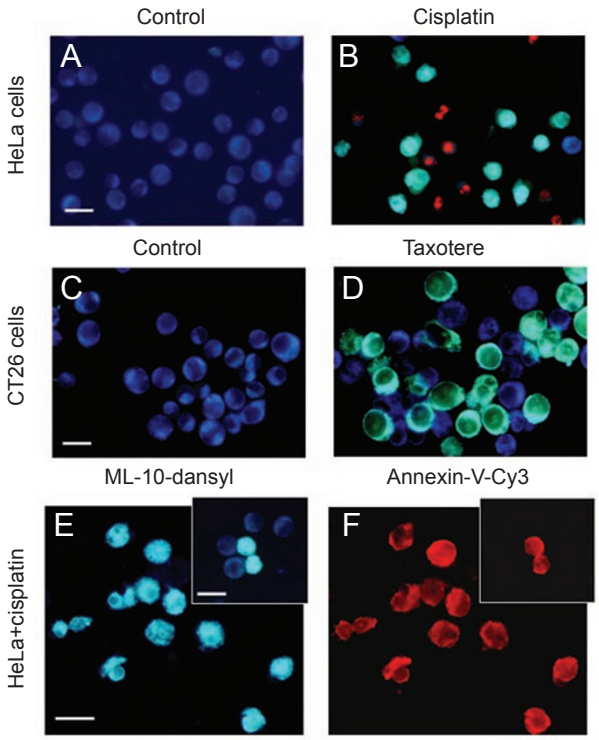

Figure 3 Detection of apoptosis by ML-10 in various cell lines and apoptotic stimuli. HeLa cells **(A**, **B**, **E**, **F)** and CT26 cells **(C**, **D)** were induced to undergo apoptosis by cisplatin (50 μM for 24 h; **B**) or taxotere (1 μM for 24 h; **D**), respectively. Cells were then co-incubated either with ML-10-dansyl and PI **(A-D)**, or with ML-10-dansyl and Annexin-V-Cy3 **(E**, **F)**, and subjected to fluorescent microscopy. Control, untreated cells did not show ML-10-dansyl uptake, and thus manifested only pale blue autofluorescence **(A**, **C)**. In contrast, induction of apoptosis was associated with emergence of numerous cells that exhibited ML-10-dansyl uptake with intracellular accumulation of the probe, reflected by the green/turquoise fluorescence of the dansyl fluorophore. ML-10-dansyl did not accumulate in PI-positive cells **(B)**, and its uptake was highly correlated with Annexin-V binding: cells that manifested ML-10-dansyl uptake were also Annexin-V-positive cells, while control viable cells did not manifest binding of either probe (**E**, **F** and respective insets).

Figure 3E and 3F). Furthermore, in these cell lines and apoptotic triggers, ML-10-dansyl did not accumulate in PI-positive dying cells (Figure 3B). These results are consistent with the observed uptake pattern of ML-10 by Jurkat cells, triggered to undergo apoptosis by Anti-Fas. Taken together, these results demonstrate the universality of the ML-10 probe as an apoptosis detector across various cell types and apoptotic triggers.

Structural/functional aspects of ML-10

We then explored the structural/functional aspects of ML-10, focusing on the potential role of the malonate moiety in the selective uptake of the tracer by apoptotic cells. For this purpose, a ^{3}H-ML-10 analog comprising only one carboxyl group (designated ^{3}H-ML-16, Figure 4) was synthesized, and its uptake into apoptotic versus intact cells was determined and compared with that of ^{3}H-ML-10. As shown in Figure 4, decarboxylation totally eliminated the selectivity of ML-10 uptake by apoptotic cells. ^{3}H-ML-16 (monocarboxylate) was not selective and accumulated similarly in both control and apoptotic cells. Therefore, the malonate moiety of ML-10 has a critical functional role, enabling selectivity in detection of apoptotic cells.

Relationship between ML-10 uptake and membrane potential

An early event of the apoptotic process is the disruption of the mitochondrial membrane potential and irreversible depolarization of the plasma membrane. These alterations are measurable by voltage-sensitive probes, such as tetramethylrhodamine-ethyl ester (TMRE) [16]. Parallel samples of Jurkat cells treated with Anti-Fas were therefore tested for ^{3}H-ML-10 uptake and TMRE fluorescence at different time points along the death process. The percentage of TMRE-positive cells and ^{3}H-ML-10 uptake levels at each time point is presented in Figure 5A. A progressive decrease in cellular TMRE fluorescence, indicative of mitochondrial membrane potential disruption, was observed with the progression of the apoptosis process. This decline in membrane potential was highly correlated with a progressive increase in ^{3}H-ML-10 uptake, creating a 'mirror image' of the time-course curve, and indicating a temporal relation between these phenomena.

Failure of mitochondrial bioenergetics during the apoptotic process is associated with permanent depolarization of the plasma membrane. Such plasma membrane depolarization (PMD) without repolarization has been described as an early molecular event in Anti-Fas-induced apoptosis [17]. We therefore investigated a possible relationship between PMD and cellular uptake of ^{3}H-ML-10. Membrane depolarization was induced in viable Jurkat cells, by incubation in K^+-rich (140 mM KCl) buffer (HBSK) in the presence of ^{3}H-ML-10, as described previously [18]. Cell viability in the K^+-rich medium throughout the time of follow-up was confirmed by negative Annexin-V binding (data not shown), in alignment with previous reports [18]. As shown in Figure 5B, depolarization was associated with a marked cellular uptake of ^{3}H-ML-10. Uptake by the depolarized Jurkat cells was time-dependent, reaching a steady state by 120 min. In contrast, non-depolarized cells showed very low ^{3}H-ML-10 uptake, which did not increase during 6 h of incubation. To further demonstrate the relationship between depolarization and tracer uptake, ^{3}H-ML-10 levels were examined during 30 and 60 min of incubation with various concentrations of extracellular potassium ($[K^+]_{ext}$), in the range of 0-140 mM (Figure 5C). Marked and linear correlations were observed throughout the examined range (r^2 = 0.9794, P = 0.00016, and r^2 = 0.9913, P = 0.000028, for the 30 and 60 min of incubation, respectively). Furthermore, the PMD-dependent uptake of ^{3}H-ML-10 could be blocked competitively by excess of non-labeled 'cold' ML-10. For that purpose, ^{3}H-ML-10 uptake was tested after 60 min of incubation with HBSK, and with various concentrations of non-labeled ML-10. A dose-dependent competitive inhibition of ^{3}H-ML-10 uptake was observed, attaining statistical significance at 0.2 mM concentration of the non-labeled compound, and reaching 50% inhibition at 1.36 mM. Taken together, these findings suggest membrane depolarization as a potential driving force for the observed selective uptake of

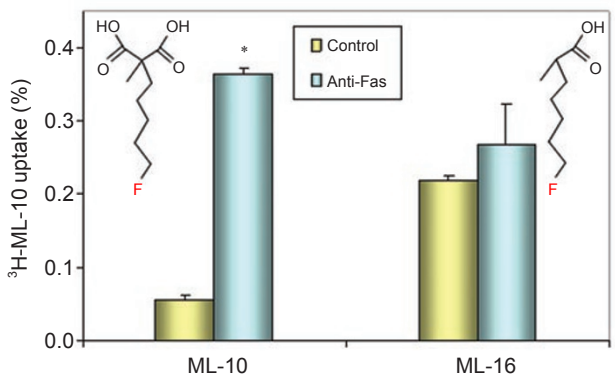

Figure 4 Structure/function considerations of ML-10: uptake of ^{3}H-ML-10 or its mono-carboxyl analog ^{3}H-ML-16 by Jurkat cells induced to undergo apoptosis by treatment with Anti-Fas versus non-treated (control) cells. As shown, decarboxylation was associated with loss of selectivity of uptake by the apoptotic cells. Values are presented as mean±SD of a representative experiment out of three performed, *P < 0.01.

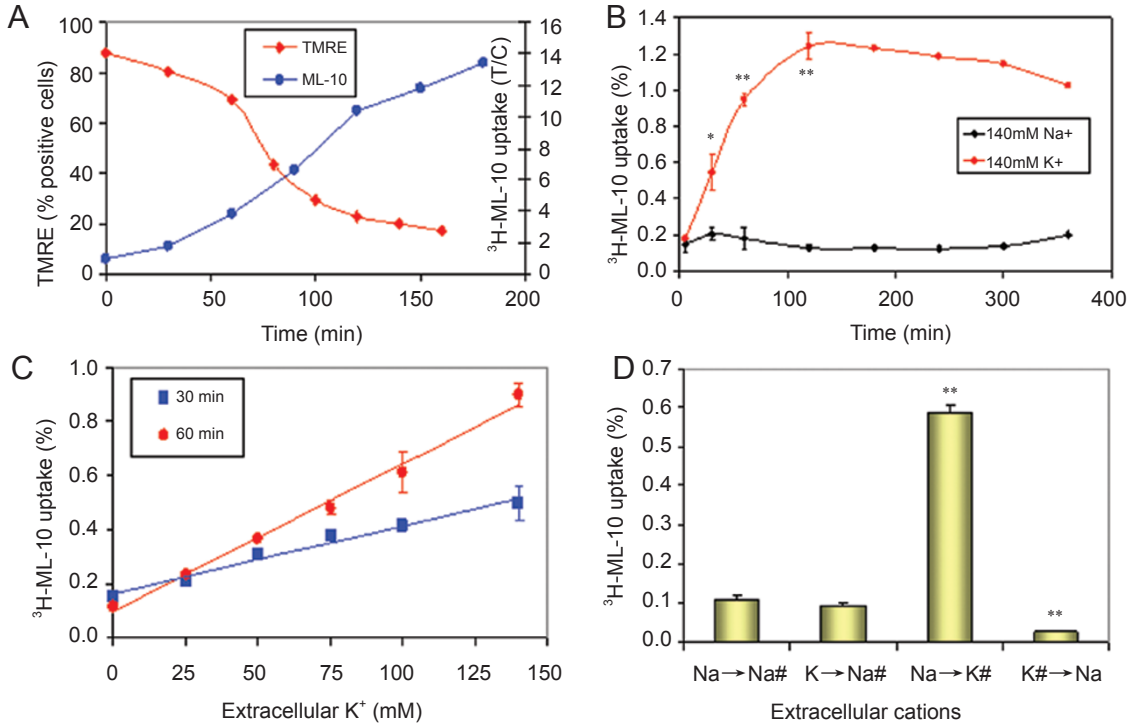

Figure 5 ^{3}H-ML-10 uptake versus membrane potential: **(A)** ^{3}H-ML-10 versus TMRE: Jurkat cells were incubated with or without Anti-Fas. At the indicated time points, ^{3}H-ML-10 uptake was determined through measurement of radioactivity. In parallel, cell samples were incubated with TMRE, and its fluorescence, as an indicator of mitochondrial membrane potential, was measured by flow cytometry. **(B)** Effect of plasma membrane depolarization (PMD) on the uptake of ^{3}H-ML-10. Depolarization was induced in viable Jurkat cells by incubation with high K^{+} buffer (HBSK), and uptake of ^{3}H-ML-10 was determined. **(C)** Linear correlation between PMD, induced by increasing extracellular concentrations of K^{+}, and uptake of ^{3}H-ML-10, evaluated at 30 and 60 min of incubation. **(D)** Reversibility of ^{3}H-ML-10 uptake upon membrane *re-polarization*. Jurkat cells were incubated in HBS or in HBSK for 60 min, and then the medium was replaced with the indicated alternate buffer for another 60 min. The # signs indicate the addition of ^{3}H-ML-10. *P < 0.05, **P < 0.01.

^{3}H-ML-10 by the cells undergoing apoptosis.

Apoptosis is characterized by *permanent* PMD, without subsequent repolarization [17]. This clearly distinguishes the PMD observed in the apoptotic cell from physiological PMD, which normally occurs, for example, in excitable cells such as neurons or myocytes, and which is very short (millisecond range) and transient, with prompt return to baseline levels. To examine whether ^{3}H-ML-10 can distinguish between *permanent* and *transient* PMD, Jurkat cells were incubated in HBSNa (containing 140 mM NaCl) or HBSK (containing 140 mM KCl) for 60 min, followed by medium replacement to the alternative buffer for another 60 min. ^{3}H-ML-10 uptake occurred simultaneously with depolarization induced by HBSK, but was completely reversible upon repolarization by the HBSNa medium (Figure 5D). Moreover, administration of ^{3}H-ML-10 at the repolarization phase after depolarization did not result in tracer uptake. These results show the *dynamic* behavior of ML-10 uptake, and therefore demonstrate its ability to distinguish between *permanent* PMD, which is characteristic of apoptotic cells, and *transient* PMD, which may be encountered physiologically.

Relationship between ML-10 uptake and cellular acidification

Cell acidification is another hallmark of apoptosis, occurring simultaneously with PMD and with apoptotic volume decrease (AVD) [19]. Acidification in apoptosis occurs both at the external membrane leaflet, due to scramblase-induced externalization of the acidic PS, and also in the cytoplasm [20]. To mimic this effect and examine its impact on ^{3}H-ML-10 uptake, ^{3}H-ML-10 uptake by viable Jurkat cells at pH 6.0 and 7.5 was measured and compared. As shown in Figure 6A, lowering the pH was associated with a marked and immediate increase in ^{3}H-ML-10 uptake, peaking at 15 min. This increase was however *transient*, as despite the constantly maintained acidic external pH (pH_{ext}) gradual decline of ^{3}H-ML-10

levels was observed, reaching near-baseline values at 120 min. This efflux of ^{3}H-ML-10 was expedited by normalization of the extracellular pH to 7.5 at 30 min. Since intracellular pH (pH_{int}) in viable cells is tightly regulated, derangement in pH_{ext} will induce adaptive mechanisms in a viable cell, resulting in normalization of pH_{int} [21]. These dynamics will therefore be reflected by an efflux of ^{3}H-ML-10. To further support this hypothesis, cells were maintained for 120 min at pH 6.0 in order to induce these putative adaptive alterations, and thereafter exposed to ^{3}H-ML-10 at that acidic pH. No increased uptake of ^{3}H-ML-10 was observed under these conditions (Figure 6B). To further substantiate the relationship between pH and ^{3}H-ML-10 uptake, cells were incubated with ^{3}H-ML-10 for 15 min at pH values ranging between 6.0 and 8.0. As shown in Figure 6C, a pH-dependent increase of ^{3}H-ML-10 uptake was observed over this range. Therefore, these results indicate both a pH_{int} dependency of ^{3}H-ML-10 uptake and *dynamic* behavior of the tracer in relation to pH_{int}. This dynamic behavior will distinguish the viable cell from its apoptotic counterpart; the induction of the physiological adaptive mechanisms to normalize the pH in the *viable cell* will render ^{3}H-ML-10 uptake to be only transient when facing altered ambient pH conditions (Figure 6A), in contrast to the apoptotic cells, which show persistent tracer retention over time (Figure 2B).

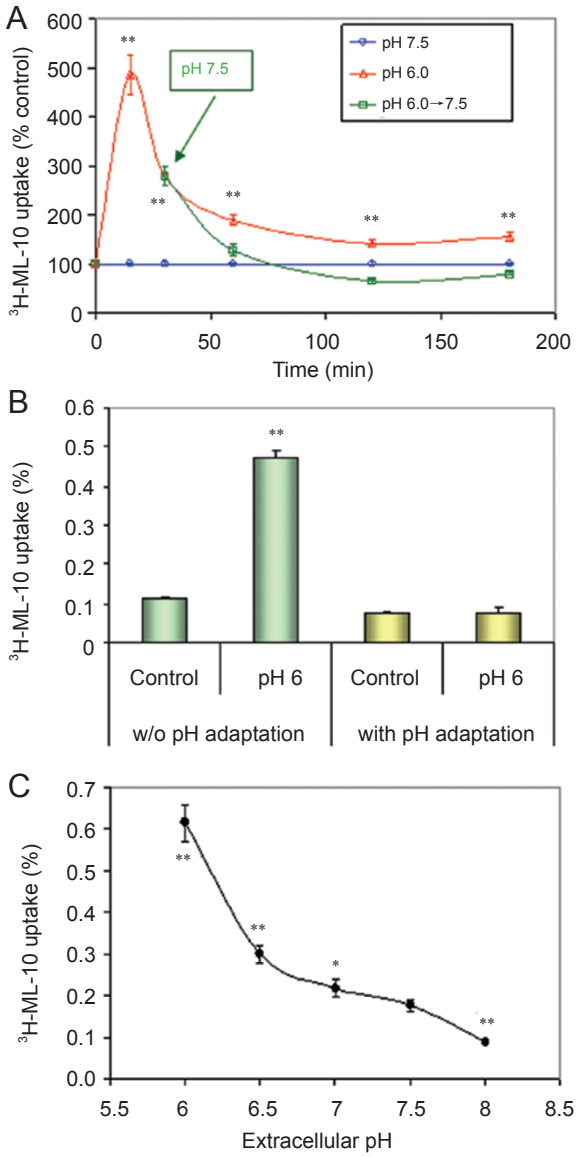

Figure 6 Effect of acidification on ^{3}H-ML-10 uptake. **(A)** The time course of ^{3}H-ML-10 uptake by viable Jurkat cells at the indicated time points following incubation in HBS at physiological pH versus uptake at pH 6.0; or at pH 6.0 with subsequent pH normalization to pH 7.5 after 30 min of incubation. **(B)** ^{3}H-ML-10 uptake by Jurkat cells without pre-adaptation to pH 6.0, compared with cells pre-adapted to pH 6.0 for 2 h. **(C)** pH dependence of ^{3}H-ML-10 uptake, at the range of extracellular pH of 6.0-8.0, at the time point of peak uptake at 15 min. Each value is the mean±SD of triplicate independent determinations from one representative experiment out of three performed, $*P < 0.05$, $**P < 0.01$.

Synergistic effect of membrane depolarization and intracellular acidification on ML-10 uptake

Since depolarization and acidification occur simultaneously during the early phases of apoptosis, we investigated the combined effect of these events on ^{3}H-ML-10 uptake. Viable Jurkat cells were incubated with ^{3}H-ML-10, and tracer uptake was examined in HBS or HBSK at either pH 7.5 or pH 6.0 (Figure 7A) over 180 min. While the control cells showed very low ^{3}H-ML-10 uptake, and the cells exposed to only PMD or acidification exhibited the same temporal profile as described above, a dramatic synergistic effect of depolarization and acidification was observed, with high uptake values detected in the HBSK-treated cells (pH 6.0), peaking at 15-30 min. Interestingly, as observed in acidification alone, the HBSK-treated cells (pH 6.0) also exhibited subsequent gradual decline of ^{3}H-ML-10 levels over the observation period. However, these levels reached those of the HBSK-treated cells (pH 7.5), and not the near-normal levels, observed over time in the cells treated with acidification alone (HBS, pH 6.0). Hence, depolarization and acidification act in remarkable synergy in promoting and augmenting ^{3}H-ML-10 uptake. These results also support the above-described *dynamic* behavior of tracer uptake in both aspects, pH and membrane potential.

To further explore this synergy of PMD and acidification in determining ^{3}H-ML-10 uptake, and to explore it in milder conditions within the physiological range, we

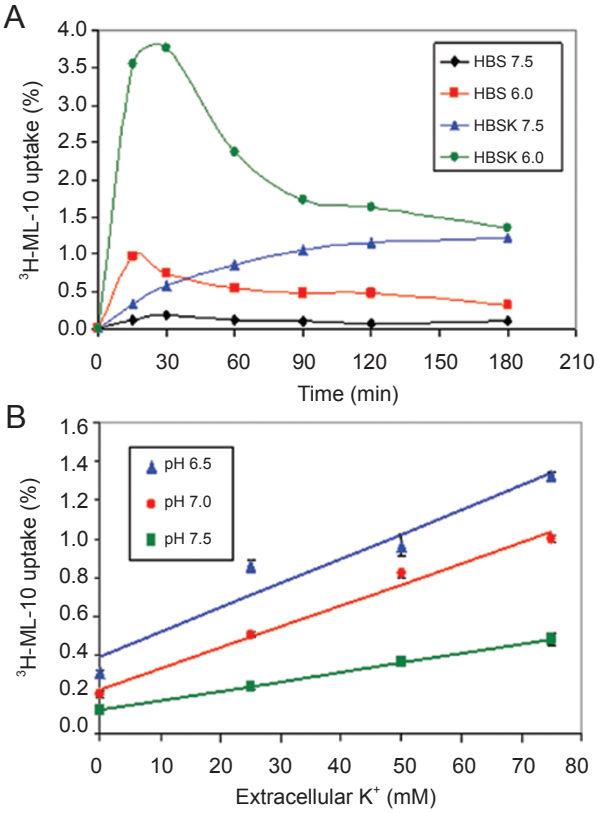

Figure 7 Synergy between depolarization and acidification in determining cellular uptake of ^{3}H-ML-10. **(A)** Concomitant depolarization and acidification: time course of ^{3}H-ML-10 uptake by Jurkat cells incubated in HBS or HBSK buffers, at pH values of 7.5 or 6.0. Each value is the mean±SD of triplicate independent determinations, from a representative experiment out of three. **(B)** Correlation between ^{3}H-ML-10 uptake and membrane depolarization, induced by high extracellular K^+ at various pH levels, mimicking the alterations in these parameters in apoptotic cells. Each value represents the mean±SEM, obtained from the sum of three independent experiments.

incubated viable Jurkat cells for 60 min in buffers with $[K^+]_{ext}$ ranging from 0 to 75 mM and at a pH range of 6.5-7.5. As shown in Figure 7B, synergy was well maintained also in these milder conditions. A linear correlation was observed between ^{3}H-ML-10 levels and the extent of depolarization (i.e., $[K^+]_{ext}$) at each of the pH levels of 7.5, 7.0 and 6.5. In addition, reduction of pH_{ext} synergistically caused augmentation of ^{3}H-ML-10 uptake. The ratio between ^{3}H-ML-10 uptake occurring in normal conditions (pH 7.5 and normal membrane potential, i.e., $[K^+]_{ext}$=0 mM) and that at pH 6.5 and moderate depolarization ($[K^+]_{ext}$=75 mM) (Figure 6B) was about 10-fold, similar to the uptake ratio observed between the apoptotic Anti-Fas-treated cells and the viable, non-treated controls (Figure 2A).

Discussion

The importance of apoptosis in the etiology or pathogenesis of numerous medical disorders, and the prospective considerable potential to improve patient care by non-invasive clinical molecular imaging of this cell death process, prompted us to develop new low-molecular-weight molecules that can serve as apoptosis detectors. Conceptually, low-molecular-weight probes can be advantageous over large proteins such as Annexin-V (MW=37 000 Da) in the aspects of radio-labeling, biodistribution and immunogenicity. Based on these considerations, we have developed and previously reported DDC [9-11] and NST-732 [12], which are members of the *ApoSense* family of recently developed small-molecule apoptosis probes. However, DDC or NST-732 do not comprise a Gla structural motif, which, as revealed in the present study, is unique in being the smallest structural motif for detection of apoptosis known to date. Indeed, ML-10 has a very compact structure, with a molecular weight of only 206 Da, and the importance of the Gla motif for its function as an apoptosis probe is demonstrated by the fact that even a minor structural modification, such as that exemplified in the 'mutated' analog ML-16 (Figure 4), caused a dramatic loss of function. The identification of such small structural motif that entails activity in selective detection of apoptotic cells is important in various aspects, as it potentially opens new avenues for attachment of diverse markers for imaging, facilitates radiolabeling for PET imaging and avenues for optimization of bio-distribution *in vivo*.

The present study introduces the concept of alkyl-malonate, derived from the Gla residue of clotting factors, as a useful structural motif for small-molecule detectors of apoptosis, and also suggests a novel mechanism for detection of apoptosis. To date, Gla has been mainly regarded as a building block of domains of clotting proteins, requiring co-operativity with other numerous adjacent Gla residues and Ca^{2+} ions, to enable protein binding to anionic phospholipid membranes. Our study provides evidence for a functional role of a single alkyl-malonate motif, in a calcium-independent mechanism, in the selective uptake into apoptotic cells.

As shown in the present study, ML-10 exhibits several features that qualify it as a detector of apoptosis. Induction of apoptosis is associated with marked increase in the cellular uptake of the probe, which is caspase-dependent and is completely blocked by caspase inhibition. ML-10 uptake occurs in parallel to the apoptotic hallmarks of Annexin-V binding and mitochondrial membrane potential disruption. Notably, this selective uptake occurs early in apoptosis, while membrane in-

tegrity is preserved, as evident by the lack of PI or TB uptake by the ML-10-positive cells. After crossing the intact, PS-externalized cell membrane, ML-10 localizes predominantly in the cytoplasm (60%) and in the nucleus (30%). Intracellular accumulation, as shown for ML-10, is potentially advantageous over binding only on the cell surface (performed, for example, by Annexin-V), as it may entail higher signal/background ratios and lack of interference with membrane function. Importantly, uptake and accumulation of ML-10 are lost upon membrane disruption. Since such disruption is one of the hallmarks of necrosis, ML-10 may be used for distinction between apoptotic and necrotic modes of cell death. In addition, these results also indicate that ML-10 is predominantly a detector of cells in *early apoptosis*, a unique feature not provided by other probes such as Annexin-V, which equally target necrotic cells, early and late apoptotic cells [22]. Detection of early apoptosis, as provided by ML-10, is of special importance, since it addresses a currently unmet need, and since these early stages are more specific for apoptosis and better related to the 'apoptosis commitment point'. Therefore, these are the target cells for future therapies for genetic or pharmacological modulation of the death process.

This profile of performance of the Gla compound ML-10 was evident in various cell lines and apoptotic triggers. In-depth characterization was performed in the present study in Jurkat cells, which were triggered to undergo apoptosis by treatment with Anti-Fas. This model system was chosen since it is a widely accepted and well-characterized model of apoptosis, utilized in numerous studies by many research groups worldwide. Importantly however, as demonstrated in the present study, an identical pattern of performance of ML-10 in detection of apoptosis was observed also with other cell lines (*e.g.* HeLa (human cervix carcinoma) cells, CT26 (murine colon carcinoma) cells) and other apoptotic stimuli, i.e., treatment with cisplatin or taxotere (Figure 3). In all these diverse cell types and pro-apoptotic triggers, ML-10 manifested the same characteristic performance, i.e., exclusion from viable cells or necrotic, PI-positive cells, selective uptake by cells in early apoptosis, intracellular accumulation, and correlation with Annexin-V binding. These observations indicate the universality of the probe as a detector of apoptosis.

The exact mechanism by which ML-10 crosses the intact, but PS-externalized cell membrane in early apoptosis remains to be elucidated. However, the malonate motif of ML-10 seems to play a key functional role, since its decarboxylation leads to a complete loss of selectivity, as evident from the studies with the closely related, decarboxylated compound ML-16. This is strikingly analogous to the clotting factors, in which inhibition of γ-carboxylation of Gla by the anticoagulant warfarin results in loss of membrane binding. Conceivably, the malonate moiety plays a role in the membrane approach of ML-10 and/or its interaction with the membrane interface, similar to the function of the Gla domain in the clotting factors.

Since charge dispersion and hydrophobicity are two major factors favoring membrane interaction of amphiphiles [23, 24, 25], the unique protonation states of alkyl-malonate may play a role in this process (Figure 8A). At physiological pH, the di-anionic form of malonate predominates, respective of the dissociation constants of the carboxylic groups of alkyl-malonic acid (pKa values of 5.8 and 2.8 in physiological conditions) [26]. However, capture of a single proton by a malonate moiety creates an acid-anion dimer, with an overall charge of -1, and with an unusual short and symmetrical internal hydrogen bond [27] (Figure 8A). Vibration of the captured proton leads to distribution of the single remaining anionic charge over the four carboxylate oxygen, thus markedly increasing ionic radius with charge dispersion [27] (Figure 8A), which in turn may act to promote interaction with the membrane interface (Figure 8B). Acidification, which is one of the hallmarks of apoptosis [19], will obviously enhance this protonation. It occurs in the apoptotic cell both at the external membrane leaflet, due to PS exposure, and at the cytoplasm, and may therefore enhance membrane interaction of ML-10. The markedly enhanced uptake of ML-10 upon acidification, as observed in our study, is in alignment with such mechanism.

Subsequently, ML-10 crosses the cell membrane to accumulate within the cytoplasm, as indicated by the results of the study. As a potential driving force for such trans-membrane movement of ML-10, our results show that ML-10 responds to membrane depolarization and also demonstrate a dramatic synergy between depolarization and acidification in promoting ML-10 uptake. These features are among the hallmarks of the apoptotic cell. Moreover, the results show a *dynamic* behavior of ML-10, upon alterations in membrane potential or pH: re-polarization led to exclusion of ML-10 from the viable cell (Figure 5D), and similarly, tracer uptake by the viable cell in response to acidification was only transient, with return to baseline levels (Figures 6A and 7A). Membrane potential and cellular pH are among the most highly regulated cellular functions in viable cells. Even excitable tissues, such as muscle fibers or neurons, are characterized by a very short depolarization in the millisecond range, with prompt return to resting potential. In contrast, apoptosis is associated with permanent loss of these vital regulatory functions [17, 19, 28]. The observed selectiv-

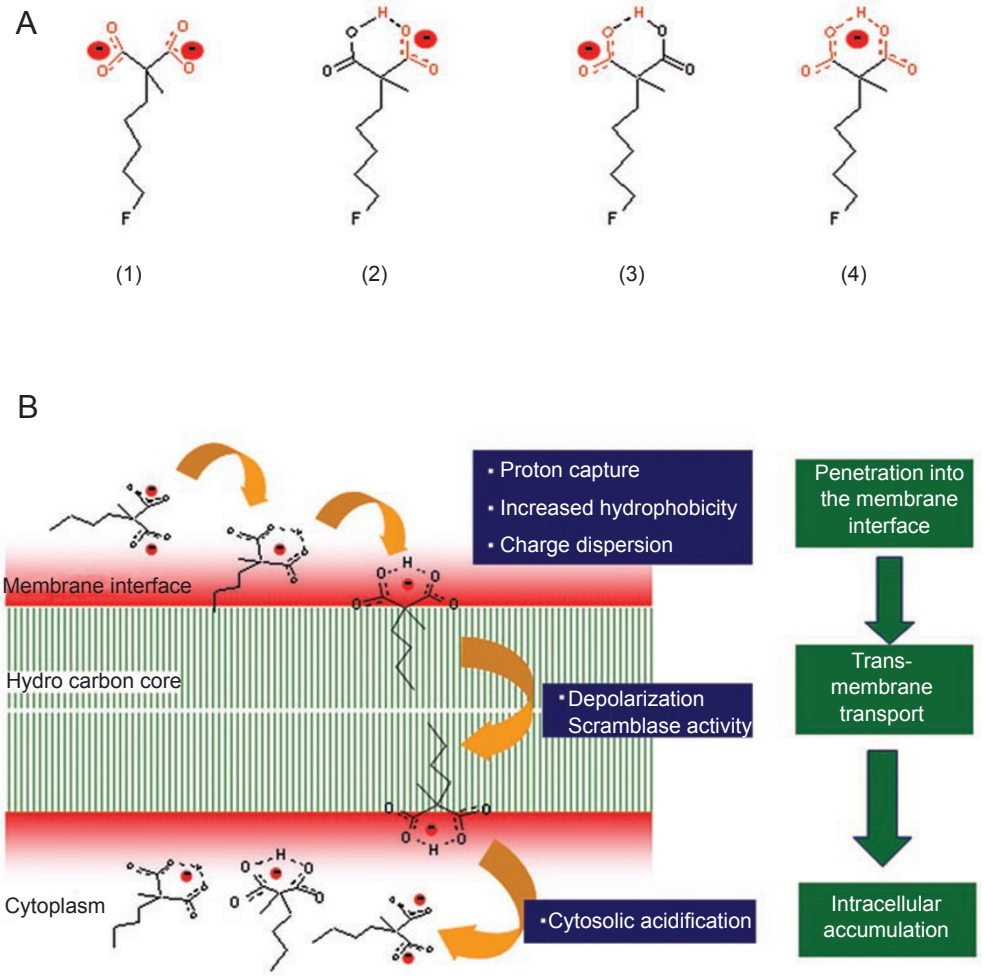

Figure 8 Potential mechanism for ML-10 uptake by apoptotic cells. **(A)** Protonation states of the malonate moiety of ML-10: (1) The di-anion form prevails in aqueous solution due to the acid dissociation constants of alkyl-malonic acid,[26] entailing high water solubility; (2 and 3) capture of a single proton will result in mono-anionic species, with a symmetrical and short internal hydrogen bond, with practical sharing of the hydrogen atom between the two carboxylates, and dispersion of the remaining negative charge over the four carboxyl oxygen atoms (4) as previously described [27]. **(B)** Proposed mechanism for the translocation of ML-10 through the intact, but depolarized, acidic and PS-exposing plasma membrane of the apoptotic cell, as observed in this study: (1) acidification of the external membrane leaflet due to PS externalization favors proton capture by the malonate moiety, with resultant increased hydrophobicity and charge dispersion, acting to facilitate penetration into the membrane interface; (2) trans-membrane passage facilitated by the depolarization, similar to that of other hydrophobic anions [23-25], and potentially assisted by activation of the membrane scramblase system; (3) sequestration in the cytoplasm, facilitated by the cytosolic acidification characteristic of apoptosis.

ity of ML-10 accumulation in the apoptotic cells can therefore be attributed, at least in part, to detection by the probe of this permanent and irreversible complex of apoptosis-related cellular alterations. Towards future use of ML-10 *in vivo*, the observation of dynamic accommodation of the probe to transient alterations in membrane potential or pH in viable cells, with ultimate exclusion from these cells, while exhibiting persistent accumulation within apoptotic cells (Figure 2B), is functionally important. Driven by the above forces, trans-membrane translocation itself can be mediated by the scramblase system activated at the membrane of apoptotic cells, membrane anionic exchanger channels (*e.g.* chloride channels [29]), organic anion transporters (*e.g.* monocarboxylate [30] or dicarboxylate carriers [31]) or through the lipid membrane itself. While the exact mechanism remains to be elucidated in future research, one potential mechanism, based on analogy to trans-membrane translocation of other hydrophobic anions [23, 24], is outlined in Figure 8B.

A major anticipated utility of ML-10 as an imaging tool may be in the development and monitoring of therapeutic effects of drugs that act by modulating the apoptotic threshold. Such therapeutic strategies are currently intensively explored worldwide for treatment of various medical disorders, such as myocardial infarction or cerebrovascular stroke. Such developments, both at pre-clinical and clinical stages, require tools for assessment of the efficacy of therapy, comparative evaluation of various candidate compounds and optimal selection of lead compounds for further development. The compact structure of ML-10, thus allowing facilitated radio-labeling, and importantly, the unique feature of ML-10 in detection of *early apoptosis*, which is currently not provided by other probes for apoptosis, may render it an attractive tool for such applications. Cells in early apoptosis, rather than necrotic or late apoptotic cells, are the main target cells for such future apoptosis-modulating drugs, and therefore, a tool for imaging of *early apoptosis*, such as ML-10, may be beneficial for such developments.

To date, successful radio-labeling of the ML-10 with the ^{18}F radio-isotope has already been performed, and the probe was successfully tested in pre-clinical animal models of apoptosis, and also in preliminary clinical trials in healthy volunteers and in patients with ischemic cerebral stroke (to be published). Performance of ML-10 in these studies *in vivo* was found to be in full agreement with the profile of activity *in vitro* as described in this study, supporting the potential future role of ML-10 for detection of apoptosis in the clinical set-up.

Materials and Methods

Synthesis of ML-10 and radio-labeling with tritium

Tert-butyl-dimethyl-silyl protected 3-butyn-1-ol was reacted with n-butyl lithium and formaldehyde to yield the pentynol derivative. The free hydroxyl group formed was converted to tosylate with tosyl chloride and potassium hydroxide. 2-Methyl-di-tert-butyl malonate was coupled with the aforementioned tosylate with the aid of potassium hexamethyl disilazane. Atmospheric pressure hydrogenation, using Lindlar's catalyst and quinoline, converted the triple to double bond in excellent yield. The silane-protecting group was removed with an acetic acid/tri-fluoro acetic acid (TFA)/water mixture at 45 °C, and the resulting alcohol was treated with mesyl chloride and tri-ethyl amine to form the mesylate. Reaction of the mesylate with tetra-butyl-ammonium fluoride in acetonitrile provided the fluoro compound in moderate yields. TFA was used to remove the protective t-butyl ester groups and to afford the formation of 2-(5-fluoro-pent-2-enyl)-2-methyl-malonic-acid. The latter was tritiated at medium pressure (4 atmos.) with the aid of palladium on charcoal catalyst, followed by HPLC purification of 2-methyl-2-(fluoro-[2,3-^{3}H]pentyl)malonic-acid (^{3}H-ML-10) with a specific activity of 50 Ci/mmol.

Synthesis of ML-10-dansyl

5-Bromopentanol was protected with dihydroxypyran catalyzed by pyridinium *p*-toluenesulfonate (PPTS), to provide 3-(5-bromo-pentyloxy)-tetrahydro-pyran. This compound was coupled with α-methyl di-*tert*-butyl-malonate with the aid of KHMDS to provide the α-methyl, THP pentyl substituted malonate. Removal of the protecting THP group was achieved in ethanol with the PPTS to yield the alcohol 2-(5-hydroxy-pentyl)-2-methyl-malonic-acid di-*tert*-butyl ester. 5-Dimethylamino-1-naphthalenesulfonamide (dansyl amide) was reacted with di-t-butyl-dicarbonate with the aid of triethylamine and small quantities of 4-dimethylaminopyridine to form *Boc*-dansyl amide. Coupling of the alcohol 2-(5-hydroxy-pentyl)-2-methyl-malonic-acid di-*tert*-butyl with the Boc-dansyl amide was achieved in a Mitsunobo reaction utilizing triphenylphosphine and diisopropyl azo-dicarboxylate. Finally, the *t*-butyl ester groups were hydrolyzed by treating with TFA at low temperature.

Cell lines and culture

Jurkat cells (human adult leukemia T-cells, clone E6-1, TIB-152), HeLa cells (human cervix carcinoma cells, CCL-2) and CT26 cells (murine colon carcinoma cells, CRL-2638) were obtained from ATCC (Rockville, MD, USA). The cells were cultured in RPMI 1640 medium (Biological Industries, Beit Haemek, Israel) supplemented with 2 mM L-glutamine, 1 mM sodium pyruvate, 100 units/ml penicillin, 100 μg/ml streptomycin and 10% FCS. Cells were maintained at 37 °C in a humidified atmosphere containing 5% CO_2.

Induction of apoptosis and necrosis

Jurkat cells at the logarithmic growth phase were harvested, counted and adjusted to 2×10^7 cells/ml in HBS, containing 10 mM Hepes in 140 mM NaCl, pH 7.5. Apoptosis was induced in the Jurkat cells by incubating the cells with IgM Anti-Fas CH11 (Medical and Biological Laboratories, Nagoya, Japan), at a concentration of 0.2 μg/ml at 37 °C in a humidified atmosphere containing 5% CO_2 for the specified periods of time. To inhibit apoptosis, 50 μM of the pan-caspase inhibitor, zVAD-fmk (Calbiochem, La Jolla, CA, USA), was added to the cells 10 min prior to the addition of the apoptotic stimuli. Necrotic cell death was induced in the Jurkat cells by three freeze and thaw cycles. To further support the universality of binding of the Gla compounds to apoptotic cells, in addition to the Jurkat cells, HeLa cells and CT26 cells were also incubated for 24 h with cisplatin (50 μM) and taxotere (1 μM), respectively, for induction of apoptosis, and then incubated with ML-10-dansyl, as described below.

Fluorescent studies with ML-10-dansyl, Annexin-V, propidium iodide (PI) and trypan blue (TB)

Following induction of apoptosis, cells (10^6 cells/ml) were incubated with ML-10-dansyl (50 μM) for 15 min at room temperature (RT), and with PI, Annexin-V labeled with fluorescein isothiocyanate (FITC, Anx-FITC) or with the Cy3 fluorophore (Anx-Cy3), according to the manufacturer's instructions (IQ products, Groningen, The Netherlands). Labeled cells were counted and photographed using a fluorescent microscope (BX51, Olympus Optical Co., London, UK), equipped with a UMNU2 filter to detect ML-10-dansyl fluorescence, a UMNIBA2 filter to detect Annexin-V-FITC, and a UMNG2 filter to detect PI and Anx-Cy3. For TB labeling, equal volumes of cell suspension and 0.5% TB solution

(Biological Industries, Beit Haemek, Israel) were mixed for 5 min, and the non-viable TB-positive and the viable TB-negative cells were counted using a hemocytometer.

Assessment of mitochondrial membrane potential by tetramethylrhodamine-ethyl-ester (TMRE)

Mitochondrial trans-membrane potential was assessed using the lipophilic voltage-sensitive dye TMRE (Molecular Probes, Eugene, OR, USA) according to the manufacturer's instructions. At the indicated time points following induction of apoptosis by Anti-Fas, Jurkat cells (3×10^5) were incubated with 100 nM TMRE for 20 min in HBS at RT. The red cellular TMRE fluorescence was analyzed using a fluorescence-activated cell sorter (FACS, Vantage VE; BD Biosciences, San Jose, CA, USA) and CellQuest software. TMRE fluorescence was excited at 488 nm and emission was measured at 580 nm.

Induction of PMD and acidification

To induce PMD, Jurkat cells were centrifuged and re-suspended in HBSK, buffered at pH 7.5 with 10 mM Hepes, in which KCl replaced NaCl at the indicated concentrations, while keeping $[Na^+]_{ext}+[K^+]_{ext}=140$ mM to maintain osmolarity. The cells were incubated in these buffers for the periods of time and buffer concentrations indicated for the specific experiment, and in the presence of ^{3}H-ML-10. To induce re-polarization of the plasma membrane, the cells were centrifuged and re-suspended in HBS containing 140 mM NaCl. To induce pH alterations, cells were incubated in HBS at different pH values, ranging from 6.0 to 8.0.

ML-10 uptake assay

At the indicated times following treatment, 2 μCi (40nmol)/ml of ^{3}H-ML-10 (50 Ci/mmol) was added to the cells and the incubation was continued for the specified periods of time (uptake time) at 37 °C. For the competition assays, non-labeled ML-10 at specified concentration was mixed with ^{3}H-ML-10. Uptake was then terminated by two cycles of centrifugation, followed by washing the cells with HBS. Cell pellets were collected in 2 × 200 μl HBS, 10 ml of scintillation fluid (Ultima Gold, Perkin-Elmer, Life and Analytical Science, MA, USA) was added, and radioactivity was determined using the liquid scintillation analyzer, Tri-CARB 2100TR (Packard Instrument Company, Meriden, CT, USA).

Caspase-3 activity measurements

Caspase-3 activity was measured using the caspase-3 fluorimetric assay kit (Sigma-Aldrich, St Louis, MO, USA) according to the manufacturer's instructions. To exclude the involvement of non-related proteases, the difference between fluorescence in the absence and presence of the specific inhibitor of caspase-3 (Ac-DEVD-CHO) was calculated. In this assay, the fluorogenic substrate of caspase-3 was composed of the fluorochrome 7-amino 4-methyl coumarin (AMC), coupled to the tetrapeptide Ac-DEVD.

Lactate dehydrogenase (LDH) leakage assay

LDH release into the medium was measured as an indicator of plasma membrane integrity, thus assisting in the distinction between apoptotic and necrotic cells. LDH activity was measured by a substrate reaction, using a colorimetric kit (cytotox 96®, Promega, Madison, WI, USA), and quantified with an ELISA reader according to the manufacturer's instructions.

Preparation of subcellular fractions

The subcellular fractions were prepared using the differential centrifugation technique [14]. Briefly, apoptotic Jurkat cells (50×10^6 cells) induced to undergo apoptosis by Anti-Fas were incubated with ^{3}H-ML-10. Cells were then washed twice with HBS, and the pellet was homogenized in 0.25 M sucrose in 50 mM Tris-HCl, pH 7.5, 25 mM KCl, and 5 mM $MgCl_2$. The nuclei were isolated by centrifugation at 800× *g* for 10 min at 4 °C. Mitochondria were isolated from the resulting supernatant by centrifugation at 8 000× *g* for 20 min at 4 °C. The resulting supernatant was then centrifuged in a micro-ultracentrifuge (M120SE, Sorvall Discovery, Kendro, USA) at 105 000× *g* for 1 h at 4 °C to yield the membrane vesicles pellet and the final cytosolic fraction. The total radioactivity in each fraction was determined, and the percent of total activity in each subcellular fraction was calculated.

Statistical analysis

Statistical analysis was performed using the unpaired Student's *t*-test (two-tailed) to evaluate the significance differences in the average values between control and treated groups. Unless stated, data are presented as mean±SD and $P < 0.05$ was considered significant. Linear regression analysis was performed using Graphpad Prism version 5.0 for Windows (Graphpad Software, San Diego, CA, USA).

Acknowledgments and Disclosure

We would like to thank Julia Dick and Mirit Argov from Aposense Ltd., Israel, for technical assistance. ML-10 is an investigational agent, developed by Aposense Ltd. (previously NeuroSurvival Technologies (NST) Ltd.).

References

1 Lahorte CM, Vanderheyden JL, Steinmetz N, Van de Wiele C, Dierckx RA, Slegers G. Apoptosis-detecting radioligands: current state of the art and future perspectives. *Eur J Nucl Med Mol Imaging* 2004; **31**:887-919.

2 Wang F, Fang W, Zhao M, *et al*. Imaging paclitaxel (chemotherapy)-induced tumor apoptosis with (99m)Tc C2A, a domain of synaptotagmin I: a preliminary study. *Nucl Med Biol* 2008; **35**:359-364.

3 Faust A, Wagner S, Law MP, *et al*. The nonpeptidyl caspase binding radioligand (S)-1-(4-(2-[18F]fluoroethoxy)-benzyl)-5-[1-(2-methoxymethylpyrrolidinyl)sulfonyl]isatin ([18F]CbR) as potential positron emission tomography-compatible apoptosis imaging agent. *Q J Nucl Med Mol Imaging* 2007; **51**:67-73.

4 Haberkorn U, Kinscherf R, Krammer PH, Mier W, Eisenhut M. Investigation of a potential scintigraphic marker of apoptosis: radioiodinated Z-Val-Ala-DL-Asp(O-methyl)-fluoromethyl ketone. *Nucl Med Biol* 2001; **28**:793-798.

5 Nelsestuen GL, Broderius M, Martin G. Role of gamma-carboxyglutamic acid. Cation specificity of prothrombin and factor X-phospholipid binding. *J Biol Chem* 1976; **251**:6886-6893.

6 Hasanbasic I, Rajotte I, Blostein M. The role of gamma-carboxylation in the anti-apoptotic function of gas6. *J Thromb Haemost* 2005; **3**:2790-2797.

7 Suttie JW. Mechanism of action of vitamin K: synthesis of

gamma-carboxyglutamic acid. *CRC Crit Rev Biochem* 1980; **8**:191-223.
8 Stirling Y. Warfarin-induced changes in procoagulant and anticoagulant proteins. *Blood Coagul Fibrinol* 1995; **6**:361-373.
9 Damianovich M, Ziv I, Heyman SN, *et al*. ApoSense: a novel technology for functional molecular imaging of cell death in models of acute renal tubular necrosis. *Eur J Nucl Med Mol Imaging* 2006; **33**:281-291.
10 Reshef A, Shirvan A, Grimberg H, *et al*. Novel molecular imaging of cell death in experimental cerebral stroke. *Brain Res* 2007; **1144**:156-164.
11 Cohen A, Ziv I, Aloya T, *et al*. Monitoring of chemotherapy-induced cell death in melanoma tumors by N,N'-didansyl-L-cystine. *Technol Cancer Res Treat* 2007; **6**:221-234.
12 Aloya R, Shirvan A, Grimberg H, *et al*. Molecular imaging of cell death *in vivo* by a novel small molecule probe. Apoptosis 2006; **11**:2089-2101.
13 Nagata S, Golstein P. The Fas death factor. *Science* 1995; **267**:1449-1456.
14 Graham JM, Sandall JK. Tissue-culture cell fractionation. Fractionation of membranes from tissue-culture cells homogenized by glycerol-induced lysis. *Biochem J* 1979; **182**:157-164.
15 Hotchkiss RS, Chang KC, Grayson MH, *et al*. Adoptive transfer of apoptotic splenocytes worsens survival, whereas adoptive transfer of necrotic splenocytes improves survival in sepsis. *Proc Natl Acad Sci USA* 2003; **100**:6724-6729.
16 Scaduto RC Jr, Grotyohann LW. Measurement of mitochondrial membrane potential using fluorescent rhodamine derivatives. *Biophys J* 1999; **76**:469-477.
17 Bortner CD, Gomez-Angelats M, Cidlowski JA. Plasma membrane depolarization without repolarization is an early molecular event in anti-Fas-induced apoptosis. *J Biol Chem* 2001; **276**:4304-4314.
18 Thompson GJ, Langlais C, Cain K, Conley EC, Cohen GM. Elevated extracellular [K^+] inhibits death-receptor- and chemical-mediated apoptosis prior to caspase activation and cytochrome c release. *Biochem J* 2001; **357**:137-145.
19 Lagadic-Gossmann D, Huc L, Lecureur V. Alterations of intracellular pH homeostasis in apoptosis: origins and roles. *Cell Death Differ* 2004; **11**:953-961.
20 Gottlieb RA, Nordberg J, Skowronski E, Babior BM. Apoptosis induced in Jurkat cells by several agents is preceded by intracellular acidification. *Proc Natl Acad Sci USA* 1996; **93**:654-658.
21 Roos A, Boron WF. Intracellular pH. *Physiol Rev* 1981; **61**:296-434.
22 Appelt U, Sheriff A, Gaipl US, Kalden JR, Voll RE, Herrmann M. Viable, apoptotic and necrotic monocytes expose phosphatidylserine: cooperative binding of the ligand Annexin V to dying but not viable cells and implications for PS-dependent clearance. *Cell Death Differ* 2005; **12**:194-196.
23 Flewelling RF, Hubbell WL. The membrane dipole potential in a total membrane potential model. Applications to hydrophobic ion interactions with membranes. *Biophys J* 1986; **49**:541-552.
24 Franklin JC, Cafiso DS. Internal electrostatic potentials in bilayers: measuring and controlling dipole potentials in lipid vesicles. *Biophys J* 1993; **65**:289-299.
25 Schamberger J, Clarke RJ. Hydrophobic ion hydration and the magnitude of the dipole potential. *Biophys J* 2002; **82**:3081-3088.
26 Smith RM, Martell AE. *Critical stability constants*. Vol 6, Suppl 2. New York and London: Plenum Press, 1984:328-333.
27 Haines TH. Anionic lipid headgroups as a proton-conducting pathway along the surface of membranes: a hypothesis. *Proc Natl Acad Sci USA* 1983; **80**:160-164.
28 Franco R, Bortner CD, Cidlowski JA. Potential roles of electrogenic ion transport and plasma membrane depolarization in apoptosis. *J Membr Biol* 2006; **209**:43-58.
29 Jentsch TJ, Stein V, Weinreich F, Zdebik AA. Molecular structure and physiological function of chloride channels. *Physiol Rev* 2002; **82**:503-568.
30 Halestrap AP, Price NT. The proton-linked monocarboxylate transporter (MCT) family: structure, function and regulation. *Biochem J* 1999; **343** Part 2:281-299.
31 Pajor AM. Molecular properties of sodium/dicarboxylate cotransporters. *J Membr Biol* 2000; **175**:1-8.